ELSEVIER

Catalysis Today 54 (1999) 531–545

CATALYSIS TODAY

www.elsevier.com/locate/cattod

Zeolite-mediated removal of NO_x by NH_3 from exhaust streams at low temperatures

M. Richter *, H. Berndt, R. Eckelt, M. Schneider, R. Fricke

Institut für Angewandte Chemie Berlin-Adlershof, Richard-Willstätter-Str. 12, D-12484 Berlin, Germany

Abstract

NH_3 stored on zeolites in the form of NH_4^+ ions easily reacts with NO to N_2 in the presence of O_2 at temperatures <373 K under dry conditions. Wet conditions require a modification of the catalyst system. It is shown that MnO_2 deposited on the external surface of zeolite Y by precipitation considerably enhances the NO_x conversion by zeolite fixed NH_4^+ ions in the presence of water at 400–430 K. Particle-size analysis, temperature-programmed reduction, textural characterization, chemical analysis, ESR and XRD gave a subtle picture of the MnO_2 phase structure. The MnO_2 is a non-stoichiometric, amorphous phase that contains minor amounts of Mn^{2+} ions. It loses O_2 upon inert heating up to 873 K, but does not crystallize or sinter. The phase is reducible by H_2 in two stages via intermediate formation of Mn_3O_4. The manufacture of extrudates preserving stored NH_4^+ ions for NO_x reduction is described. It was found that MnO_2 can oxidize NO by bulk oxygen. This enables the reduction of NO to N_2 by the zeolitic NH_4^+ ions without gas-phase oxygen for limited time periods. The composite catalyst retains storage capacity for both, oxygen and NH_4^+ ions despite the presence of moisture and allows short-term reduction of NO without gaseous O_2 or additional reductants. The catalyst is likewise suitable for steady-state $DeNO_x$ operation at higher space velocities if gaseous NH_3 is permanently supplied. ©1999 Elsevier Science B.V. All rights reserved.

Keywords: NO_x removal; Zeolites; Ammonia storage; Manganese oxide; Egg-shell deposition

1. Introduction

We could show, in a preceding article [1], that ammonium ions fixed to microporous alumino silicates are capable of reducing NO_x to N_2, at temperatures as low as 343 K, at moderate space velocities. A process was proposed, named catalytic low-temperature conversion (CLTC) of NO_x, where temporary NO_x emissions are abated without addition of a reductant for limited time periods. Exploiting the pronounced storage capability of the catalyst system for NH_3 at low temperatures and the high reactivity towards NO_x, a cyclic reaction/regeneration is feasible. The reaction requires an intermediary oxidation of NO to NO_2 and obeys the overall equation (Z^- denotes the anionic zeolite framework):

$$4Z^-NZ_4^+ + 4NO + O_2 \rightarrow 4N_2 + 6H_2O + 4Z^-H^+ \quad (1)$$

Here, NH_4^+ ions are stoichiometrically consumed while the zeolite is being converted into its protonic form [2]. Temporary emissions of NO_x could thus be removed without gaseous reductants if an appropriate amount of catalyst is applied. The NH_4^+ ions can be replenished by contacting the zeolite with NH_3, either in situ at the temperature of reaction or ex situ at ambient conditions. Cyclic operation with alternating NH_3 storage and NO_x reduction offers advantages

* Corresponding author. Tel.: +49-30-6392-4343; fax: +49-30-6392-4392.

PII: S0920-5861(99)00215-1

for the process control of the SCR from stationary sources as it is not necessary to dose low amounts of ammonia permanently into a catalyst bed with the risk of undesired slip of the toxic reductant.

Whereas the NH_3 uptake by the zeolite satisfactorily operates under dry and wet conditions, the presence of water considerably inhibits the NO_x conversion to N_2. It was argued that the interaction of NO with the zeolite surface, which is a necessary step to initiate oxidation to NO_2 by gaseous oxygen, is inhibited by adsorbed water. Therefore, an additional oxidation component seems to be necessary to ensure adequate rates of NO oxidation in the presence of water. From the literature it is known that manganese oxides either as pure components or loaded on alumina are suitable catalysts for the continuous conversion of NO_x by ammonia at moderate temperatures [3–8]. Hence, we tried to combine the parent zeolite Y with Mn(IV) oxide, but to keep the storage properties of the zeolite for NH_3 and the accessibility of the ${NH_4}^+$ ions within the micropores. Aluminium-rich zeolites like zeolite Y in their protonic or ammonium form (H or NH_4 form, respectively) are susceptible to dealumination when calcined at temperatures of 700 K or higher [10]. Therefore, the exchange of Na^+ by ${NH_4}^+$ ions has to be performed as the final step of the preparation route. For this purpose, a specific method of generation of a MnO_2 phase on the external surface of the zeolite (egg-shell deposition) has been developed. The Mn(IV) oxide phase deposited on the zeolite was characterized by several techniques to gain insight into textural and morphological details. The CLTC of NO by ${NH_4}^+$ ions in a wet feed was studied in a transient mode at temperatures in the 313–443 K range.

2. Experimental

2.1. Catalyst preparation

A commercial zeolite Y (Si/Al = 2.3) was supplied in its alkali (NaY) or ammonium (NH_4Y) form by Aldrich. The theoretical composition of the material (Na form) is $Na_{58}(Al_{58}Si_{134}O_{384})\cdot 240\ H_2O$ [10]. For precipitation of the MnO_2 phase, solutions of Mn(II) acetate tetrahydrate (purissimum, Merck) and potassium permanganate were used. To ensure a uniform precipitation, the parent zeolite was sieved to a particle-size fraction <100 μm before modification. One recipe for loading zeolite NaY with an amount of 15 wt.% MnO_2 reads as follows: 15 g of the zeolite powder were suspended in 50 cm^3 water and the suspension was vigorously stirred at room temperature. To this suspension 2.45 g Mn(II) acetate were added. Then, 50 cm^3 of a 0.13-molar $KMnO_4$ solution were added under continuous stirring. The colour of the solution immediately turned to dark brown, indicating formation and precipitation of MnO_2 according to Eq. (2).

$$3Mn^{2+} + 2{MnO_4}^- + 2H_2O \rightarrow 5MnO_2 \downarrow + 4H^+ \tag{2}$$

Finally, the suspension was heated to 353 K and kept for a further 30 min at this temperature. The zeolite powder was then filtered and dried. Manufacturing of the catalyst involved two further preparation steps. First, a silica binder was added to the MnNaY zeolite, and the wet material was shaped to extrudates (4-mm diameter) and calcined. This yielded sufficient mechanical strength of the extrudates so as to allow further handling. Second, the Na^+ ions had to be replaced by ${NH_4}^+$ ions which was achieved by ion exchange with an ammonium sulphate solution. The pH during the exchange is slightly acidic (ca. 4). The pellets remain intact during the ion exchange. Since treatments at higher temperatures would diminish the capacity of the catalyst for NO_x conversion due to thermal NH_3 desorption, the catalyst pellets were only dried at 453–473 K after completion of the exchange.

Fig. 1 visualizes the preparation method and approximate dimensions of the composite catalyst, in part anticipating results of the characterization study.

For catalytic measurements, the extrudates were crushed and particles of 0.35–0.70 mm size were sieved out for further use. Sample designation will be abbreviated, including percentage of Mn (expressed as MnO_2), state of the zeolite (H, NH_4 or Na form) and calcination temperature (as subscript given in K). Binder content is marked by addition of the letter B. Data on the investigated samples and their composition are summarized in Table 1.

The catalysts were analyzed by OES-ICP analysis at various stages of preparation. The modified zeolite NaY, aimed at 15 wt.% MnO_2 loading (9.6 wt.% Mn), had the following composition after calcination at 773

Table 1
Investigated samples

Sample designation	Composition	Remarks
$15MnNaY_{423}$	85 wt% NaY, 15 wt.% MnO_x	dried at 423 K
$15MnNaY_{773}$	85 wt% NaY, 15 wt.% MnO_x	calcined at 773 K
$15MnNaY_{873}$	85 wt% NaY, 15 wt.% MnO_x	calcined at 873 K
$15MnNH_4Y_{773}$-B	75 wt% NaY, 15 wt.% MnO_x, 15 wt.% SiO_2	from sample $15MnNaY_{773}$
$15MnNH_4Y_{873}$-B	75 wt% NaY, 15 wt.% MnO_x, 15 wt.% SiO_2	from sample $15MnNaY_{873}$

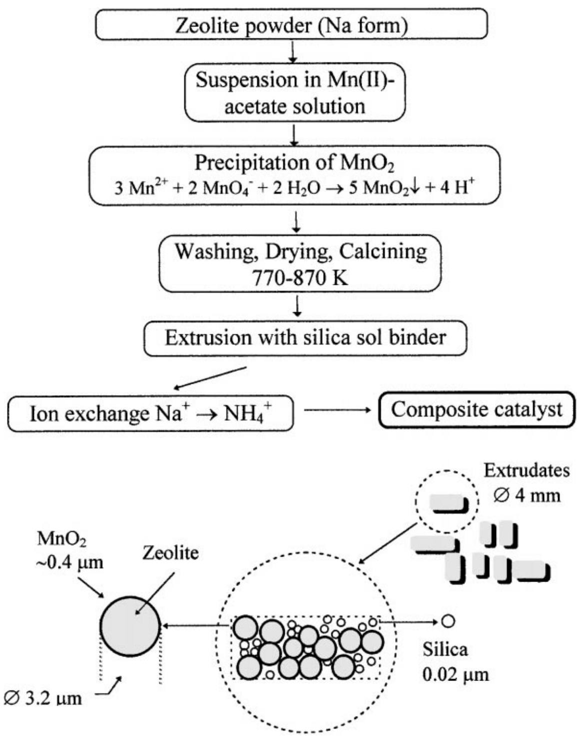

Fig. 1. Scheme of catalyst preparation and approximate dimensions of extruded composites.

K: 23.7 wt.% Si, 8.9 wt.% Al, 6.5 wt.% Na, 1.8 wt.% K, 9.6 wt.% Mn, remainder O. Potassium was not contained in the parent zeolite, but was introduced during precipitation from the $KMnO_4$ solution used. It is reported in Ref. [11] that up to 2 wt.% potassium could be included in the precipitate. It was confirmed by a final check of the extrudates following NH_4^+ ion exchange that ca. 75% of the K^+ ions are exchangeable by NH_4^+ ions. The same exchange extent followed for Na^+ ions. Obviously, ca. 35% of the zeolitic Na^+ ions cannot be exchanged by NH_4^+ ions upon completion of the catalyst preparation. This is attributed to a partial blockage of zeolite pores by MnO_2 precipitated on the zeolite as will be shown in Section 3.2. The storage capacity of the zeolitic component for NH_4^+ ions amounts to 3.3 $mmol^{-1}$ $g_{zeolite}$ as calculated from chemical analysis.

2.2. Characterization

The analytical composition of the sample was determined by optical emission spectroscopy with excitation by inductively coupled plasma (OES-ICP) with the spectrometer Optima 3000 XL (Perkin–Elmer).

Pore volumes and surface areas were determined by nitrogen adsorption on the ASAP 2010 M facility (Micromeritics). Calculation of pore size followed the method of Barrett–Joyner–Halender (BJH) [12] according to implemented software routines.

Particle-size analysis was done on a Fritzsch particle sizer Analysette 22, equipped with an He–Ne laser (wavelength 632.8 nm) according to methodical standards. The sample was suspended in an aqueous solution of $Na_4P_2O_7$.

Thermogravimetric analysis was performed on a TG/DTA 92 derivatograph (Setaram). The sample was held at room temperature for 5 min and then heated up to 1073 K at a rate of 10 K min^{-1}.

A Bruker E 500 spectrometer was used to measure the ESR spectra in X-band at 77 K and at room temperature. The detailed conditions of sample pretreatment are given in Section 3.

XRD measurements were performed by a Guinier–Lenne focussing camera (Nonius) with film displacement using CuKα radiation. Reference XRD pattern for zeolite Y was taken from literature data bases.

Temperature-programmed reduction (TPR) was performed applying the characterization system

AMI-1 (Altamira) equipped with a thermal conductivity detector. For reduction, a feed of 5 vol.% H_2 in Ar was used at a heating rate of $10\,K\,min^{-1}$. The overall flow rate amounted to $0.5\,cm^3\,s^{-1}$. The consumption of H_2 could be determined from the integrated peak areas by calibration with argon pulses into the H_2/Ar flow.

^{27}Al MAS NMR spectra were measured on a UNITYplus-500 spectrometer (VARIAN) at 130.1 MHz. The spinning rate was 10.7 KHz. Two thousand scans were accumulated with a relaxation delay of 1 s. Chemical shifts are related to a $[Al(OH)_6]Cl_3$ solution.

2.3. Catalytic measurements

The catalytic measurements were performed in a flow system equipped with an integral flow reactor (i.d. 10 mm) and an on-line sampling system. The feed was premixed from diluted NO (0.1 vol.% in He), pure O_2, He and, optionally, NH_3 (5 vol.% in He); all gases supplied by Messer Griesheim, by mass flow meters and a four-channel multi-controller (147B) from MKS Instruments. Water was introduced into the carrier gas by a saturator held at the desired temperature by a thermostat.

Unless otherwise specified, the feed consisted of 1000 ppm NO, 10 vol.% O_2 and helium as diluent. The standard space velocity (GHSV) amounted to $2000\,h^{-1}$ ($3.6\,cm^3$ catalyst volume). After the reaction had been started at the desired temperature, it was followed as a function of the process time. The sampling frequency was 10 min at minimum.

Analysis of the product flow was conducted by gas chromatography (HP 6890 series) on two parallel capillary columns, Poraplot Q, $25\,m \times 0.53\,mm$, and molecular sieve 5A, $25\,m \times 0.53\,mm$, with an additional HayeSep Q precolumn and back-flush to vent. For simultaneous detection, two TCD were installed allowing the identification of NO, N_2, O_2, H_2O, NH_3, CO and CO_2. Analysis was managed by the ChemStation software (HP). Simultaneously, the exit stream composition was continuously analyzed by a Maihak Multigas sensor, including a catalytic converter delivering NO and NO_2 values besides CO_2, O_2 and H_2O concentrations.

3. Results and discussion

3.1. CLTC of NO_x

The conversion of 1000 ppm NO in the presence of 10 vol.% O_2 over non-modified zeolite NH_4Y in the temperature range 323–463 K was investigated using a dry feed and a wet feed (7 vol% water added). Results are summarized in Fig. 2.

With dry feed, >90% conversion of NO is achieved at temperatures lower than 373 K (GHSV = $2000\,h^{-1}$). The conversion of NO_x declines at higher temperatures although the reservoir of NH_4^+ ions is high enough as followed from stoichiometric considerations. Presumably, this negative temperature dependence is associated with the shift of the adsorption equilibrium of NO. The equilibrium constant of NO adsorption decreases with temperature and limits the rate of reaction which involves the intermediary oxidation of NO to NO_2. The mechanism proposed in Ref. [1] emphasized the similarity to the diazotation of primary amines by nitrous acid. NO and NO_2 form N_2O_3 at low temperatures which, in turn, is in equilibrium with HNO_2 according to Eq. (3).

$$N_2O_3 + H_2O \leftrightarrow 2HNO_2 \quad (3)$$

Water is present in the adsorbed form (note that the samples after the ion exchange Na^+ by NH_4^+ were only dried at mild temperatures not exceeding 473 K). Furthermore, H_2O formed during the reaction is accumulated on the zeolite up to saturation. Conversion of NO_x is considerably less effective with wet feed

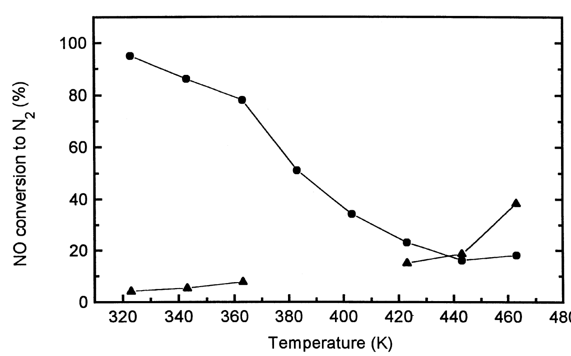

Fig. 2. NO_x conversion over zeolite NH_4Y and temperature dependence under dry and wet conditions. 1000 ppm NO, 10 vol.% O_2, (●) dry feed, (▲) wet feed (7 vol.% H_2O), GHSV = $2000\,h^{-1}$.

(cf. Fig. 2). Nearly no conversion is observed at reaction temperatures <373 K. At 463 K, the conversion degree amounts to 40%. The range between 363 and 423 K was not analyzed, because no semi-steady-state values could be obtained. It was evident, that beneath 373 K capillary condensation of water inside the zeolite micropores prevailed. Evaporation of water at temperatures >373 K induces a sharp overshooting of N_2 formation. Obviously, the reaction turns from a three-phase path (including liquid nitrous acid) to the two-phase gas–solid reaction within this transitional temperature regime. Therefore, reaction temperatures for the NO_x abatement within wet feed has to be chosen somewhat higher than 373 K. It should be noted, that the conversion increases with higher temperatures. It is concluded that the presence of water modifies the rate of NO oxidation preventing adsorption of NO on the surface at low temperatures. Consequently, the equilibrium of NO adsorption is shifted to the gas phase, thus the temperature dependence of the equilibrium constant does not disguise the temperature dependence of the rate constant. Although this interpretation is based on qualitative arguments, the conclusion drawn has proved successful.

Starting from the approach that the initial oxidation of NO by gaseous O_2 is a crucial reaction step suppressed by moisture, we tried to improve the oxidation properties of the zeolite by a metal oxide promotor. After initial screening of several oxides, it turned out that MnO_2 is the best promotor. The optimum loading was found to be ca. 15 wt.%.

3.2. Characterization of the composite catalysts

3.2.1. Surface area and pore volumes

Characteristic data are summarized in Table 2. Physisorption measurements include initial thermal evacuation of the samples at 723 K. Because of its limited thermal stability, thermal evacuation of sample NH_4Y was performed at 473 K for 3 h.

Table 2
Textural characterization of zeolite Y and catalyst $15MnNaY_{773}$

	NH_4Y	NaY	$15MnNaY_{773}$
S_{BET} ($m^2\,g^{-1}$)	641	928	608
S_{micro} ($m^2\,g^{-1}$)	607	922	546
V_{micro} ($cm^3\,g^{-1}$)	0.29	0.44	0.26
V_{macro} ($cm^3\,g^{-1}$)	0.04	0.01	0.17

Both, NH_4Y and NaY are commercial products, differing in surface area and micropore volume considerably. This may be associated with the ion-exchange process necessary for manufacturing the ammonium form. Nevertheless, textural properties of NH_4Y are in agreement with literature data (cf., e.g. Ref. [13]). Loading of zeolite NaY with 15 wt.% MnO_2 leads to significant changes of the surface area and the micropore volume of the zeolite. Even if one takes into account that sample 15MnNaY contains 15% MnO_2, the loss in micropore volume and surface area is around 30%. Whereas the non-modified zeolite contains mainly micropores, the binder-free modified zeolite reveals a considerable part of macropores. The latter is obviously introduced by the oxidic Mn phase.

3.2.2. Particle-size analysis

Both, NaY_{773} and $15MnNaY_{773}$ were characterized in terms of their particle size. From geometrical considerations it had to be expected that the uniform deposition of 15 wt.% MnO_2 should lead to a detectable increase in crystallite size. Results of particle-size analysis are shown in Fig. 3. Particle sizes follow a logarithmic normal distribution [14] (dotted lines) with good accuracy. The most frequent particle diameter is significantly shifted from 2.1 to 3.2 μm after modification of NaY with MnO_2. This increase is reconcilable with the estimated thickness of MnO_2 deposited as egg-shell on the zeolite crystallites. Pictures taken by a light microscope could verify that the precipitation of MnO_2 has not introduced agglomeration of crystals or formation of separate Mn oxide particles. The external surface areas (i.e. geometrical surface areas) of samples NaY_{773} and $15MnNaY_{773}$ are 3.7 and 2.6 $m^2\,cm^{-3}$, respectively. Reasonably, the outer surface area is lower at higher particle sizes. The percentage of outer surface area amounts to ≈10% of the overall surface area accounting for an apparent density of the material of 0.55 $cm^3\,g^{-1}$ (cf. Table 2).

3.2.3. X-ray analysis of the MnO_2 phase

XRD pattern of samples $15MnNaY_{423}$, $15MnNaY_{773}$ and $15MnNaY_{873}$ show only the diffraction pattern of the zeolite structure. The pattern of zeolite NaY remains unchanged despite calcination. This confirms

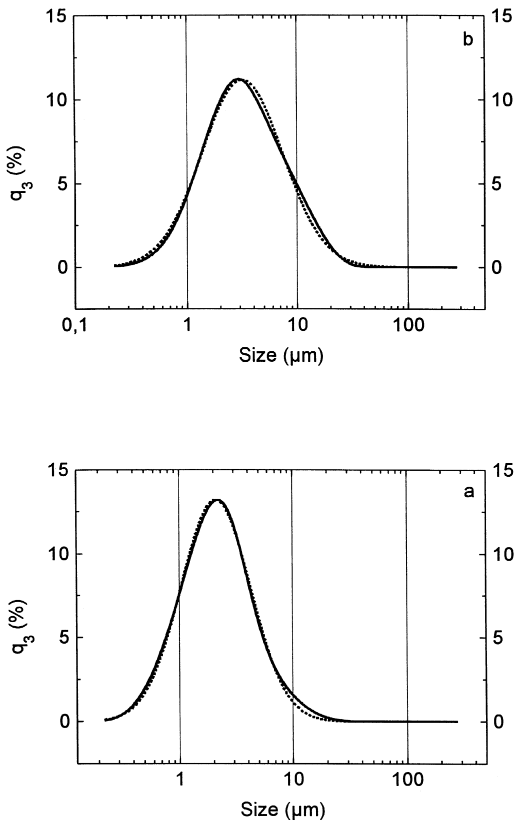

Fig. 3. Results of particle-size analysis for non-modified NaY (a) and $15MnNaY_{773}$ (b). Density distribution q_3 (%). Dotted curve indicates fitting by a logarithmic normal distribution.

the relative thermal stability of the zeolite Y in the Na form. Crystalline Mn oxides are not present either in the sample calcined at 423 K or in samples calcined at higher temperatures. This means that the amorphous MnO_2 phase is stable against crystallization processes.

3.2.4. Thermoanalysis

TG and DTA curves are shown in Fig. 4 for the sample $15MnNaY_{423}$. The TG profile is dominated by an overall weight loss of nearly 15% between room temperature and 1073 K, caused by the endothermic water desorption occurring up to ca. 773 K. However, no additional thermal effect was observed indicating any crystallization process.

3.2.5. Temperature-programmed reduction

The reducibility of samples $15MnNaY_{423}$, $15MnNaY_{773}$ and $15MnNaY_{873}$ is demonstrated in Fig. 5 (a–c), respectively. The total hydrogen consumption determined from the overall peak areas is listed in Table 3. The TPR profiles of all three samples show two reduction peaks up to a reduction temperature of 773 K. A further minor H_2 consumption is observed above 800 K for the samples calcined at 773 and 873 K which points to the existence of small MnO_2 amounts stabilized by interaction with the zeolite matrix.

The reduction of a stoichiometric MnO_2 phase to MnO would require 1750 μmol $H_2{}^{-1}$ g_{cat}. However,

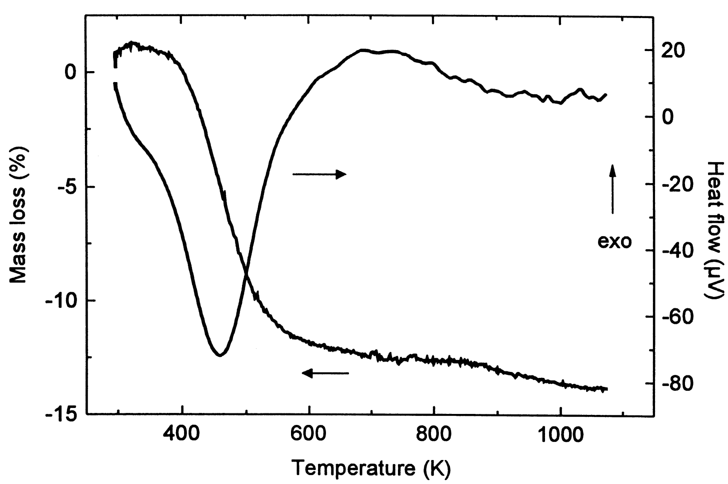

Fig. 4. Thermoanalysis of sample $15MnNaY_{423}$. Heating rate 10 K min^{-1}. Sample weight 21.66 mg.

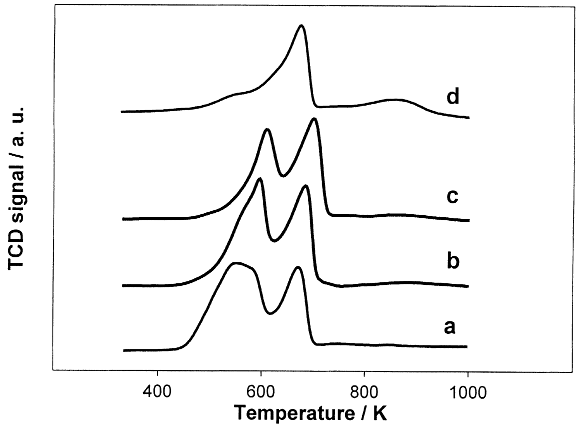

Fig. 5. Reduction profiles of sample $15MnNaY_{423}$ (a), $15MnNaY_{773}$ (b) and $15MnNaY_{873}$ (c) and $15MnNaY_{773}$ after treatment with NO up to 773 K (d). Conditions: 5 vol.% H_2 in Ar, flow rate $0.5\,cm^3\,s^{-1}$, heating rate $10\,K\,min^{-1}$.

Table 3
TPR results

Sample	H_2 consumption ($\mu mol\,g^{-1}$)	Composition of the initial MnO_x phase[a]
15 $MnNaY_{423}$	1300	$MnO_{1.74}$
15 $MnNaY_{773}$	1250	$MnO_{1.71}$
15 $MnNaY_{873}$	1090	$MnO_{1.62}$
15 $MnNaY_{773}$[b]	910	$MnO_{1.51}$

[a] Calculated from H_2 consumption.
[b] Pre-treated by NO.

the hydrogen consumption measured on all 15MnNaY samples is lower and decreases with increasing calcination temperature. Obviously, the MnO_2 phase has a non-stoichiometric composition, i. e. there is an oxygen deficiency that increases with higher calcination temperatures.

The two-peak pattern of reduction as well as the location of peak maxima on the temperature axis are in good agreement with results in Ref. [4] for MnO_x loaded on Al_2O_3. It should be noted, however, that the Mn phase loaded on a non-zeolitic support by impregnation and subsequent calcination is determined by the kind of Mn salt used, the textural properties of the support and the calcination procedure [4]. Characteristically, the reduction of MnO_2 bulk oxide proceeds in two stages via intermediary formation of Mn_3O_4 [3], according to

$$3MnO_2 + 2H_2 \rightarrow Mn_3O_4 + 2H_2O \qquad (4)$$

$$Mn_3O_4 + H_2 \rightarrow 3MnO + H_2O \qquad (5)$$

Therefore, the ratio of the first and second TPR peak areas should be 2 : 1. In order to separate the two reduction steps, the overall TPR profile of sample $MnNaY_{773}$ was deconvoluted into two peaks using commercial peak fitting software. The significant lower peak area ratio of 1.15 confirms the oxygen deficiency of the MnO_2 phase on the catalyst samples. This deficiency is more pronounced for samples calcined at higher temperatures. Temperature-programmed heating of sample $15MnNaY_{423}$ in inert atmosphere showed that oxygen is released at temperatures higher than 673 K. The amount determined up to a temperature of 873 K was ca. 290 $\mu mol\,g^{-1}$ and is compatible with the $MnO_{1.62}$ composition calculated for the sample $15MnNaY_{873}$ from TPR results. Consequently, the phase has to be viewed as a non-stoichiometric MnO_x phase with $1 < x \le 2$.

Additionally, the question has been addressed how far NO is oxidizable by bulk oxygen of the MnO_x phase. An attempt was made to arrive at an answer by TPR experiments using NO as reductant. For this purpose, sample $15MnNaY_{773}$ was heated up to 773 K in a helium flow containing 5000 ppm NO at a heating rate of $10\,K\,min^{-1}$ and held at the final temperature for 45 min. The attempt to observe NO_2, thus produced, by mass spectrometric analysis was not successful. Because it could not be excluded that NO_2, though formed, had been retained within the connection lines to the mass spectrometer, sample 15MnNaY773 was eluted by an argon flow at 773 K, cooled down to 423 K and, subsequently, subjected to TPR with H_2 at standard conditions. The result of this experiment is included in Fig. 5 (profile d). The first reduction peak is drastically decreased and, therefore, the H_2 consumption is significantly lowered (cf. Table 3). Obviously, the MnO_x phase has been partially reduced by NO.

3.2.6. Electron spin resonance

It is known that MnO_2 prepared by precipitation according to Eq. (2) contains a certain percentage of Mn^{2+} ions that are relatively resistant against oxidation [13]. This is one reason why the average valence state of the manganese is lower than four in such products. The non-stoichiometry of the MnO_2 phase precipitated on zeolite Y became evident even from the

TPR measurements described before. ESR measurements should reveal the existence of Mn^{2+} ions and, above all, the fate of these ions during catalysis. Therefore, sample 15MnNH$_4$Y$_{773}$-B was characterized before, and after, catalysis (see later). ESR spectra have been taken at 77 and 293 K after evacuation at room temperature. Results are shown in Fig. 6. It is worth mentioning that a variation of temperature of the ESR measurement (293 and 77 K) had nearly no influence on the shape of the spectra. The spectrum (Fig. 6(a)) of the fresh sample 15MnNH$_4$Y$_{773}$-B is characterized by six strong and narrow hyperfine structure (hfs) lines resulting from Mn^{2+} ions with a nuclear spin of $I = 5/2$. The parameters are $g = 2.008$ and $A = 95.6$ G. The high resolution of the signal can be taken as strong evidence for the presence of isolated Mn^{2+} species. However, in addition to the hfs, a broad line of low intensity is superimposed which originates from interacting Mn^{2+} ions.

The ESR spectrum of the sample after use in the CLTC reaction for several hours (Fig. 6(b)) reveals nearly no hfs, i.e. the concentration of isolated Mn^{2+} species is dramatically decreased. The intensity of the broad line of interacting Mn^{2+} ions is estimated to be about tenfold lower than that observed for the fresh sample.

The reason for the disappearance of the Mn^{2+} ESR signal or its decrease of intensity can be the oxidation as well as reduction of the paramagnetic species. Reduction of existent Mn^{2+} species to lower valence states during catalysis is unlikely. However, it has to

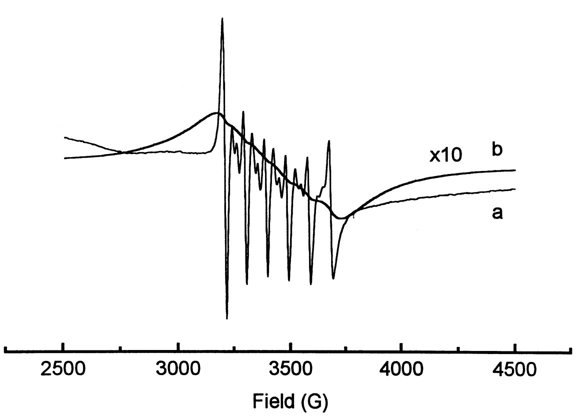

Fig. 6. ESR spectra of sample 15MnNaY$_{773}$-B, fresh (a), used (b) (catalysis at 403 K for ca. 9 h).

be taken into consideration that the mean valence state of the manganese after sample preparation is between 3 and 4. Reduction of Mn^{3+} or Mn^{4+} during reaction should lead to an increase of the concentration of Mn^{2+} ions. Due to the high concentration of manganese in the catalyst (15% MnO_2) this has a twofold effect: first, the concentration of isolated Mn^{2+} ions decreases (which is reflected by the ESR spectrum) and, second, the dipole–dipole interaction of adjacent Mn^{2+} ions increases which leads to signal broadening until ultimately a spectrum could not be obtained at all.

3.3. Catalytic properties

3.3.1. NO_x conversion over composite MnO_x/NH_4Y under wet conditions

A representative example characterizing the performance of the composite catalyst in wet exhaust gas is shown in Fig. 7. At a reaction temperature of 403 K, complete conversion of 1000 ppm NO_x at

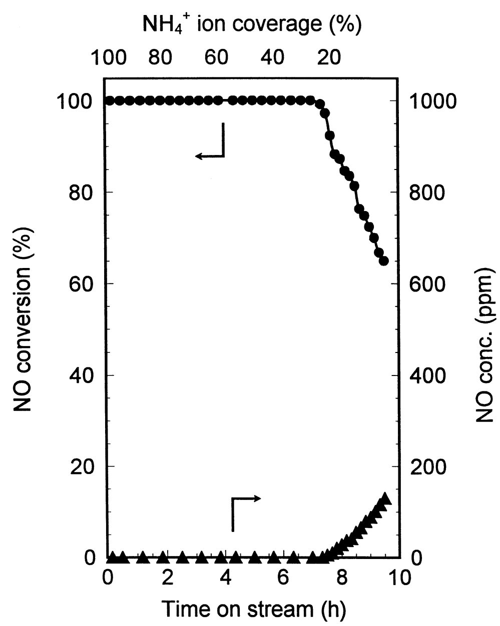

Fig. 7. NO_x conversion to N_2 over the composite catalyst 15MnNH$_4$Y$_{773}$-B under wet conditions vs. reaction time. Reaction conditions: temperature 403 K; feed: 1000 ppm NO, 10 vol.% O_2, 7 vol.% H_2O; space velocity = 2000 h^{-1}. Decrease of NH_4^+ coverage with time-on-stream on top. (●) Conversion of NO to N_2 (%), (▲) NO concentration (ppm).

a GHSV of $2000\,h^{-1}$ is maintained over 7 h without reductant addition. The reactant inlet amounts to 5.35×10^{-3} mmol min^{-1} and requires the same molar amount of NH_4^+ ions to become reduced according to Eq. (1).

The experiment runs over 1.8 g of catalyst so that a total concentration of 4.19 mmol NH_4^+ ions is available. The consumption is as high as 5.35×10^{-3} mmol min^{-1}. Theoretically, the stored NH_4^+ ions guarantee 100% conversion over nearly 13 h. This time is shortened to ca. 9 h, taking into account the loss of accessible zeolite pore volume of 30% due to the precipitation of MnO_x. The latter estimation is reconcilable with the experimental results. With each hour of full conversion the NH_4^+ ion coverage is diminished by ca. 10%. The conversion of NO_x tends to fall already below 100% at a residual NH_4^+ ion coverage of 20–25%. Disregarding some uncertainties associated with numerical estimation, the mode of NO breakthrough and decrease of N_2 formation points to a kinetic limitation. It is reasonable to assume that not all of the NH_4^+ ions are equally accessible and the involvement of those not easy to reach by the reactant slow down the rate of reaction at low NH_4^+ coverage. This is not necessarily a consequence of the preparation route. Rather it is associated with the zeolite structure Y per se, where four crystallographic different framework sites exist for the fixation of NH_4^+ ions [10]. It is reasonable that not all sites are equally accessible for NO_x in the CLTC reaction.

Reaction temperatures <400 K do not allow complete reduction of NO_x. One experiment, starting at 363 K and increasing the reaction temperature successively by 20 K every hour, reached 15% conversion at 363 K, 45–50% at 383 K and >95% at 403 K. The catalyst suffers some deterioration by this mode of operation. Nevertheless, complete NO_x conversion can be achieved by enhancement of the reaction temperature to 425 K. A graphical representation of this type of characterization is given in Fig. 8 for modified reaction conditions (500 ppm NO, GHSV $4000\,h^{-1}$). This means the same NO inlet (5.35×10^{-3} mmol min^{-1}) as in Fig. 7 (1000 ppm NO, GHSV = $2000\,h^{-1}$), but a shorter mean residence time (1/GHSV). At the shorter residence time, complete conversion of NO requires a reaction temperature of 423 K whereas, at 403 K, 75–80% of NO is converted to N_2.

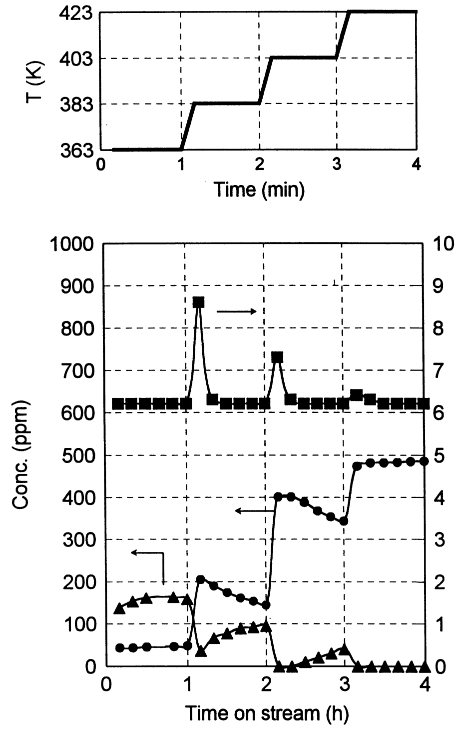

Fig. 8. NO_x conversion in wet exhaust over the composite catalyst $15MnNH_4Y_{773}$ at the temperature schedule shown on top. Conditions: 500 ppm NO; 10 vol.% O_2; 7 vol.% H_2O; carrier gas He; GHSV = $4000\,h^{-1}$. (■) H_2O (vol.%), (●) N_2 (ppm), (▲) NO (ppm).

Two points should be emphasized. The temperature increase from one level to the next is complete within 10 min and new isothermal conditions are established. Apart from the desorption of water, an overshooting of the N_2 concentration at a new temperature level was observed. This overshooting is not attributable to a temperature overshooting but, obviously, to the decomposition of intermediates partially stored on the catalyst surface. During each temperature increase, a part of the intermediate decomposes to N_2 besides that part produced by the pseudo-steady-state reaction. The accumulation of intermediates not immediately reacting to N_2 may be the actual reason for the (reversible) deactivation. The temporal course of the water concentration in the gas phase reflects the superimposition by water desorbing from the surface upon a temperature increase. This effect is weaker at higher temperatures, where less H_2O is retained on the catalyst surface.

3.3.2. NH_3 storage capacity

The applied precipitation of MnO_2 on the suspended zeolite crystallites of nearly 3 μm in size leads to an egg-shell loading of a thin but uniform, amorphous, non-stochiometric MnO_2 phase containing some isolated Mn^{2+} ions. Whereas the NH_3 storage capability of zeolites is well known, the contribution of the MnO_x phase to fixation of NH_3 is not evident. For clarification, the contribution of zeolitic NH_4^+ ions to the CLTC of NO was excluded using sample $15MnNaY_{773}$-B (Fig. 9). The reaction was started by admixture of 1000 ppm NH_3 to the feed of 1000 ppm NO, 10 vol.% O_2 and 7 vol.% water. After steady-state conversion the supply of NH_3 was cut off. The transient decline of N_2 formation informs on the amount of NH_3 stored on the MnO_x phase. The area under the curve corresponds to a concentration of 0.07 mmol NH_3 per gram of catalyst. The overall capacity of stored NH_3 on the composite catalyst $15MnNH_4Y_{773}$-B was checked by the CLTC reaction itself using dry feed. Accordingly, a NO concentration of 5000 ppm was reacted with the catalyst in the presence of 10 vol.% O_2 at 383 K until no further N_2 formation occurred. The N_2 formed corresponds to the usable concentration of NH_4^+ ions which was found to amount to 1.7 mmol g^{-1}. Two conclusions can be drawn. First, the amount of NH_3 fixed to the MnO_x is <5% of the overall amount related to unit weight of catalyst. Second, the percentage of NH_4^+ ions available for the conversion of NO_x on the composite catalyst is lower than that calculated on the basis of the zeolite content (70 wt.%), being 2.31 mmol per gram of the catalyst. Thus, nearly 25% of the calculated overall NH_4^+ ion concentration could not be utilized. Obviously, the MnO_2 shell covers pore entrances of the zeolite microcrystals, thus limiting the access of reactants to the interior. This conclusion is in line with results of the chemical analysis discussed before, namely that the exchange of Na^+ ions by NH_4^+ ions is limited to ca. 65% for the composite catalyst. Thus, a loss of usable NH_4^+ ion capacity for transient NO_x conversion is inherent to the preparation procedure.

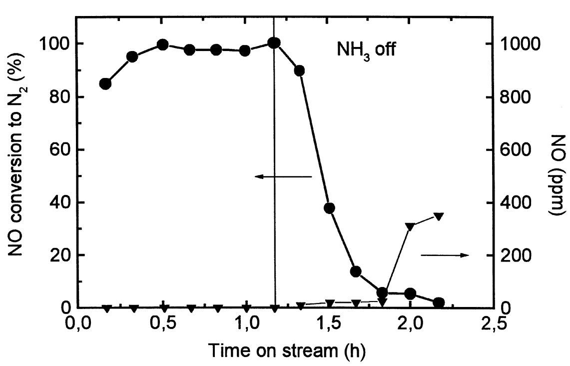

Fig. 9. NO_x conversion vs. time-on-stream over sample $15MnNaY_{773}$-B at 403 K. Feed: 1000 ppm NO; 10 vol.% O_2; 7 vol.% H_2O; 1000 ppm NH_3. GHSV = 2000 h^{-1}. At 1.2 h time-on-stream the NH_3 supply was cut off. (●) NO conversion to N_2 (%), left side, (▲) NO concentration (ppm), right side.

3.3.3. Influence of gas-phase oxygen

The reaction over non-modified NH_4^+ zeolites does not proceed at all without gas-phase oxygen, because the initial oxidation of NO to NO_2 is an indispensable reaction step. This is, however, not the case for the MnO_x/NH_4Y composite catalyst that is able to convert NO to N_2, also without gas-phase oxygen. This is shown in Fig. 10 for the sample $15MnNH_4Y_{873}$-B. The reaction sequence was as follows: the sample was heated in a He stream to the reaction temperature of 403 K in dry atmosphere and, afterwards, equilibrated

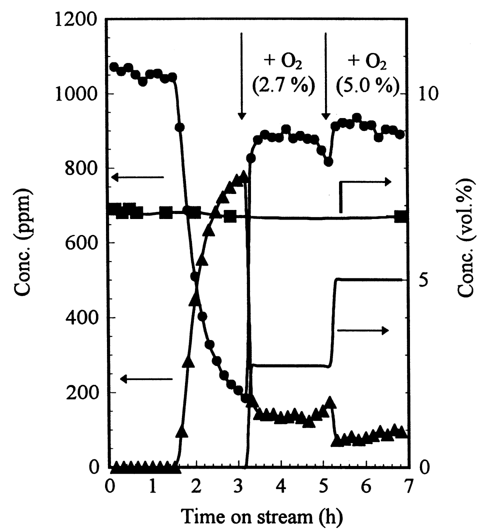

Fig. 10. Conversion of NO (1000 ppm) to N_2 over $15MnNH_4Y_{873}$-B in wet exhaust (7 vol.% H_2O) at 403 K vs. time-on-stream without gas-phase oxygen (0–3 h), in the presence of 2.7 vol.% O_2 (3–5 h), and 5 vol.% O_2 (5–7 h). Reductant: NH_4^+ ions of the zeolite component. Space velocity 2000 h^{-1}. (■) H_2O (vol.%), (●) N_2 (ppm), (▲) NO (ppm), (solid line) O_2 (vol.%).

with 7 vol.% H_2O. Once the partial pressure of water in the gas phase became constant, the NO/He stream was switched on. Although the reaction was performed without gas-phase oxygen, complete conversion of NO to N_2 is observed (1000 ppm N_2) over nearly 90 min before the conversion declines and NO is detected in the gas phase. This decline of NO conversion is not caused by the exhaustion of the NH_4^+ ions because, in the presence of gas-phase oxygen the reaction proceeds for more than 7 h at full conversion (cf. Fig. 7). Therefore, the decline of NO conversion must be related to properties of the MnO_x phase. It is evident that the NO is oxidized by oxygen of the MnO_x phase. The MnO_x contains oxygen easily removable by NO even after calcination at 873 K where it has lost already some of its oxygen by thermal desorption (cf. Table 3).

When oxygen is admixed (2.5 vol.%) after 180 min time-on-stream, the NO conversion immediately increases from 20% to nearly 90% where a pseudo-steady-state can be maintained for nearly one hour before the conversion starts to decline again reaching nearly 80% within a time interval of 30 min. Further enhancement of the oxygen content (5 vol.%) again increases the NO conversion to 90%. At 10 vol.% O_2 (not shown) complete conversion can be re-established. The same behaviour is observed for sample 15MnNH$_4$Y$_{773}$-B, where the oxygen consumable by NO is somewhat higher, as has been inferred from a comparison of the N_2 formed during the transient period.

3.3.4. Cyclic operation

One example for cyclic operation is shown in Fig. 11. The criterion chosen for turning to NH_3 reload was the breakthrough of 100–150 ppm of NO at the reactor exit. Starting with sample 15MnNH$_4$Y$_{773}$-B, the formation of 1000 ppm N_2 indicates full conversion. First reload of NH_3 was done after 4.5 h time-on-stream for 30 min at the reaction temperature. Resuming the reaction, a complete conversion of NO is achieved again, but the breakthrough of NO to the limit of 150 ppm occurs somewhat earlier than observed for the first reaction cycle. This seems to indicate a certain loss of NH_3 storage capacity to occur during reaction. It is known that zeolites tend to become dealuminated, at least partially, under hydrothermal

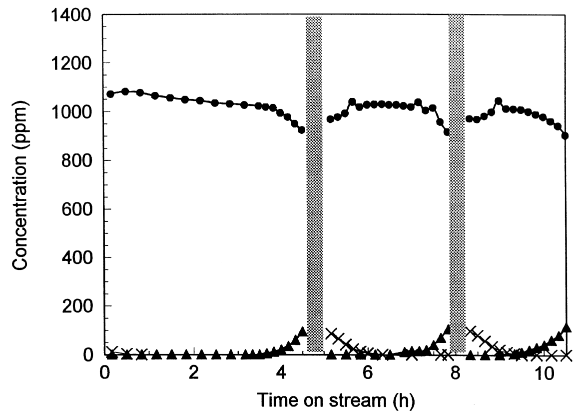

Fig. 11. Cyclic NO_x conversion and NH_3 adsorption on catalyst 15MnNH$_4$Y$_{773}$-B (0.8 g) at 423 K. Feed: 1000 ppm NO; 10 vol.% O_2; 7 vol.% H_2O (reaction); GHSV = 4000 h^{-1} and 0.75 vol.% NH_3/He; flow rate 2 cm^3 s^{-1} (shaded bars in situ regeneration), (●) N_2, (▲) NO, (×) N_2O.

conditions. Transformation of tetrahedrally coordinated framework aluminium into octahedrally coordinated non-framework species would mean a loss of Brønsted acid sites and, hence, of active sites for NH_3 fixation. For evaluation, sample 15MnNH$_4$Y$_{773}$-B was checked before, and after, cyclic DeNO$_x$ operation by ^{27}Al MAS NMR spectroscopy. Spectra are shown in Fig. 12, including the parent NaY zeolite. The intense signal at ca. 60 ppm originates from tetrahedrally coordinated framework aluminium. Octahedrally coordinated (non-framework) aluminium leads to a signal at ca. 0 ppm. Comparing spectra Fig. 12 (a–c) allows us to conclude the following:

1. the commercial NaY zeolite is well crystallized and does not contain any detectable non-framework aluminium;
2. the preparation of sample 15MnNH$_4$Y$_{773}$-B including calcination and ion exchange ($Na^+ \rightarrow NH_4^+$) has not caused dealumination of the framework; and
3. the cyclic DeNO$_x$ operation in the presence of 7 vol.% water vapour is accompanied by a slight dealumination of the zeolite framework.

The percentage of non-framework aluminium species after 12 h time-on-stream is estimated to be ca. 10%.

A further detail of the cyclic operation is that immediately after the switch over from He–H_2O–NH_3 to He–H_2O–NO–O_2 (where the reactor is flushed with pure He before changing the feed), a transient

Table 4
Comparison of essential features for commercial NH_3-SCR processes and the CLTC route of NO_x abatement

	CLTC of NO_x	SCR of NO_x
Catalyst	zeolite (NH_4form) + MnO_2	oxides (TiO_2/V_2O_5, MoO_3, WO_3)
Working temperature	<373 K (dry feed) 373–473 K (wet feed)	473–673 K
Process conditions	cyclic operation preferred	continuous operation
Storage capacity of the catalyst for NH_3	high	low
Constancy of NO_x/NH_3 ratio	not critical due to storage properties	important
Undesired side products	none	N_2O
Selectivity of reductant utilization	=100%	≤100%

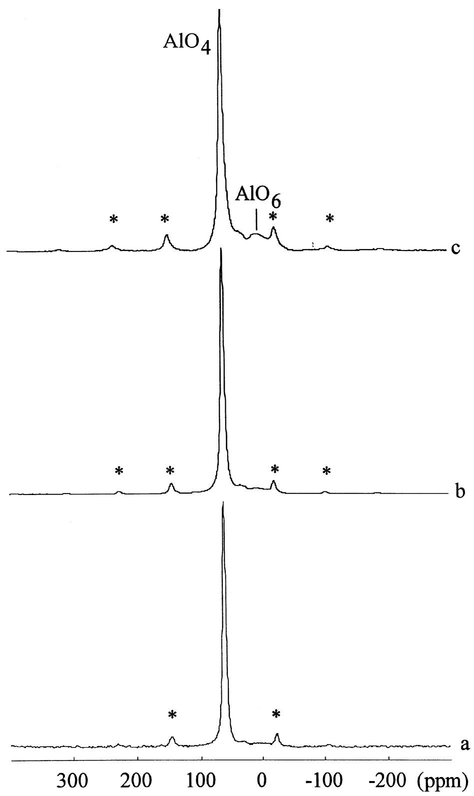

Fig. 12. ^{27}Al MAS NMR spectra of (a) NaY as received, (b) sample 15MnNH$_4$Y$_{773}$-B before reaction and (c) sample 15MnNH$_4$Y$_{773}$-B after cyclic CLTC operation for 12 h. (*) denotes spinning sidebands.

formation of small amount of N_2O is observed. Probably, NO_2 reacts in the presence of oxygen with ammonia stored on Lewis sites of the zeolite to ammonium nitrate during the reload. Ammonium nitrate decomposes into N_2O under reaction conditions. Formation of N_2O, however, is not observed during reaction between NO_x and NH_4^+ ions. The advantage of the CLTC process in comparison to the established SCR process with permanent addition of the reductant NH_3 is given in Table 4.

3.3.5. Steady-state operation

Catalysts for abatement of NO_x from exhaust gases of stationary sources have to operate at space velocities exceeding 10 000 h^{-1}. A cyclic mode of operation at comparable NO_x inlet concentrations with exclusive utilization of stored ammonia as reductant would require very short cycle periods. From the viewpoint of process design, this would be a drawback. Therefore, it was of interest to find out whether the composite catalysts can be operated at higher space velocities with a permanent supply of ammonia. Representative results are shown in Fig. 13. Measurements were performed with samples 15MnNH$_4$Y$_{773}$-B and 15MnNaY$_{773}$-B at a GHSV of 12 000 h^{-1} (28 800 $cm^3\,g^{-1}\,h^{-1}$) within the temperature range of 403 to 453 K. The feed included 1000 ppm of NH_3 besides 1000 ppm NO, 10 vol.% O_2 and, optionally, 7 vol.% H_2O. In order to differentiate between the contribution of inherent NH_4^+ ions of sample 15MnNH$_4$Y$_{773}$-B and supplied gaseous NH_3, the same experiments were repeated with sample 15MnNaY$_{773}$-B which does not contain any NH_4^+ ions after preparation. The conclusion to be drawn from Fig. 13 is that the composite catalyst achieves NO_x conversions >90% at reaction temperatures >440 K under wet conditions. Sample 15MnNH$_4$Y$_{773}$-B keeps NO_x conversion 10 to 15 points higher than that achieved by sample 15MnNaY$_{773}$-B. This implies that the NH_4^+ ions present in sample 15MnNH$_4$Y$_{773}$-B have a beneficial influence on the catalyst performance. Reference measurements with dry feed at 403 K revealed conversion extents of NO to N_2 higher than 90% for both samples.

Measurements are in progress to extend the space velocities to even higher values. Preliminary comparisons with a commercial SCR catalyst (V_2O_5–WO_3/TiO_2) revealed a considerably lower activity of the latter at comparable conditions.

3.3.6. Mechanistic considerations

Eng and Bartholomew [15,16] reported results on the NO_x reduction by NH_3 over H forms of zeolites ZSM-5, mordenite and Y in a semi-steady state operation, i. e. with pre-adsorbed ammonia as reductant. An activation energy of the conversion of NO_x on H mordenite (Si/Al = 5) with ammonia pre-adsorbed at 595–625 K was determined by a formal first-order approach as amounting to 56.4 kJ mol^{-1}. The authors found comparable values for the reaction performed over H-ZSM-5 [15] and cited further reference data from the literature confirming apparent activation energies within the range of 50–60 kJ mol^{-1} for dry feed.

Kinetic constants derived from own results presented in Fig. 8 by the same first-order approach obeyed the Arrhenius relation as shown in Fig. 14. The rate of NO conversion was formulated according to Eq. (6).

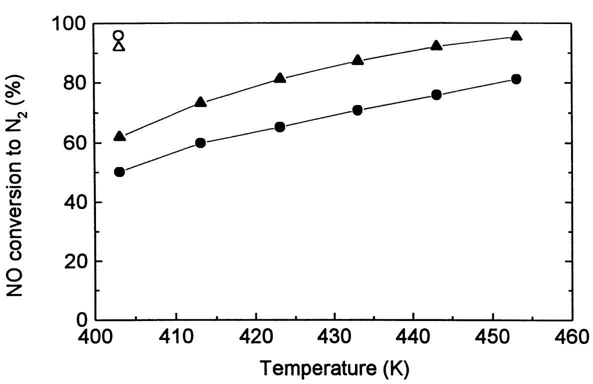

Fig. 13. NO conversion to N_2 vs. reaction temperatures with dry (open symbols) and wet (filled symbols) feed. Samples $15MnNH_4Y_{773}$-B (triangles) and $15MnNaY_{773}$-B (circles). Permanent supply of 1000 ppm NH_3. GHSV = 12 000 h^{-1} (28 800 cm^3 g^{-1} h^{-1}). Feed 1000 ppm NO, 10 vol.% O_2, optionally 7 vol.% H_2O.

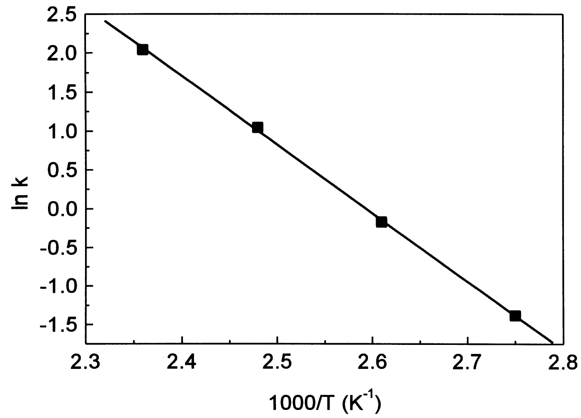

Fig. 14. Arrhenius diagram for rate constant, k_{obs} (s^{-1}), of assumed first-order NO conversion to N_2. Apparent activation energy, 75 kJ mol^{-1}. Data and conditions cf. Fig. 8.

$$r_{NO} = \frac{dc_{NO}}{dt} = -k\vartheta_{NH_4^+} c_{NO}^n c_{O_2}^m \tag{6}$$

where $\vartheta_{NH_4^+}$ denotes the surface coverage with NH_4^+ ions, and c_{NO}, c_{O_2} are the gas-phase concentrations with reaction orders n and m, respectively. The equation is simplified by assuming that all components except NO are in excess and remain unchanged during reaction. The rate constant, k, is modified to the observed value, k_{obs}, including numerical contributions from the inherent assumptions, Eq. (7)

$$k_{obs} = -(v/m)\ln(1-\alpha) \tag{7}$$

with v is the flow rate (cm^3 s^{-1}), m the catalyst mass (g), and α the NO conversion to N_2.

The activation energy yielded a value of ca. 75 kJ mol^{-1} which is somewhat higher than reported in Ref. [15,16] for pure zeolites and dry feed. Nevertheless, the value is still reasonable, taking into account the modified catalyst structure and the presence of water. Moreover, the reaction kinetics at low temperatures is probably superimposed by adsorption processes of reactants or intermediates which is not accounted for in the assumed kinetics. Ammonia, fixed as NH_4^+ to the zeolitic Brønsted acid sites, is not displaced by H_2O. NO does not adsorb on MnO_x/Al_2O_3 in any significant amounts in the absence of oxygen [5], whereas the adsorption in the presence of O_2 indicates that NO needs to be converted to NO_2 for fixation. Inhibition by water is ascribed to a surface hydroxylation of both, the MnO_x phase and the Al_2O_3 carrier. The hydroxylation of MnO_x is more pronounced at low loadings (2 wt.% or less) and the inhibiting effect of water decreased at higher Mn loadings [6]. The egg-shell character of the Mn-modified zeolite Y, with a comparably high amount of MnO_x, prevents obviously extended surface hydroxylation and helps to oxidize the NO during its passage through the porous MnO_x providing NO/NO_2 in appropriate relation to the zeolite interior for reaction with NH_4^+ ions. The oxidation of NO on the MnO_x shell is possible both, by gas-phase oxygen or by participation of MnO_x bulk oxygen.

Oxidation of NO by bulk oxygen of manganese oxides has not been reported so far. On the contrary, Kapteijn et al. [3] claimed that oxygen of manganese oxides does not participate in the SCR reaction. This apparent discrepancy is readily explained by considering the different nature of the precipitated MnO_x phase and the materials used by Kapteijn et al. Certainly, crystalline MnO_2 is more difficult to reduce than the non-stoichiometric amorphous MnO_x phase prepared by precipitation on the zeolite matrix.

Another discrepancy to own results is the observation made by Eng and Bartholomew [15] that zeolite HY is not active in the SCR of NO_x by NH_3 despite its high concentration of acid sites. The authors suggested that the super cages of the zeolite structure Y allows abundant fixation of NH_3 in a less favourable configuration than on other investigated zeolites (ZSM-5, mordenite), thus preventing catalytic reduction of incoming NO_x. However, we could show in Ref. [1], and in the present work (cf. e.g. Fig. 2), that the zeolite structure Y can be used for conversion of NO_x by pre-adsorbed ammonia (or starting right with the ammonium form of the zeolite) at temperatures of around 373 K in the absence of gaseous H_2O. A plausible explanation is that the thermal treatment of zeolite HY at higher temperatures ($T > 625$ K), as performed by Eng and Bartholomew [16] severely deteriorated the crystallinity of the zeolite.

Regarding the mode of NH_3 activation on supported manganese oxides, intermediates other than NH_4^+ ions have been proposed in the literature as well. Kijlstra et al. [8], for example, suggested amide species as reactive intermediates, formed from adsorbed NH_3 on MnO_x/Al_2O_3 catalysts at low temperatures. From IR spectroscopic measurements, the authors conclude that NH_4^+ ions are only formed to a minor extent on the Al_2O_3 support. This is reasonable since neither of the catalyst components contain strong Brønsted acid sites. We could prove in Ref. [1] by NH_3 TPD before, and after, CLTC reaction that NH_4^+ ions of the zeolite are doubtless utilized for reduction of NO_x. Results presented in Fig. 9 of the present work revealed the existence of activated NH_3 even on the MnO_x phase. The $DeNO_x$ activity of sample $15MnNaY_{773}$-B that cannot form NH_4^+ ions on the zeolite component also prove that MnO_x can accomplish the reaction by itself in the presence of gaseous NH_3. On the basis of the catalytic results, it cannot be ruled out that activation of NH_3 on the MnO_x shell proceeds in a different way to that on the zeolite component. For clarification, further measurements are necessary.

4. Conclusions

The characterization of the zeolite modified by precipitation of 15 wt.% MnO_2 revealed that the microcrystals have been covered with a thin shell of amorphous, non-stoichiometric, macroporous MnO_x that has beneficial influence on the multi-stage conversion of NO to N_2 in wet gas by NH_4^+ ions fixed to the zeolite framework. The MnO_x phase ensures fast NO oxidation in a wet atmosphere at low temperatures (403 K), thereby accelerating the overall process of NO_x reduction to N_2. At higher space velocities, a permanent supply of gaseous NH_3 is one alternative to avoid short cycle periods of reaction/regeneration. It could be shown that the composite catalyst operates satisfactorily at a GHSV of 12 000 h^{-1} (28 000 $cm^3\,g^{-1}\,h^{-1}$). The detected dealumination of the zeolite component due to the presence of moisture seems to limit the long-term stability of the composite catalyst. This apparent drawback can be overcome by using the alkali form of the zeolite for steady-state operation. The MnO_x phase by itself is able to accomplish the $DeNO_x$ process when NH_3 is permanently supplied. However, the performance of this variant of SCR catalyst results in less active catalysts. Nevertheless, the performance compares better to the conventional SCR catalysts based on V_2O_5–WO_3/TiO_2 at temperatures <473 K. The influence of other exhaust components has yet to be clarified. The kind of MnO_x phase precipitated on the zeolite crystals is of paramount importance. Other catalyst formulations, consisting of mechanical mixtures of various manganese oxides (MnO, Mn_2O_3, Mn_3O_4, MnO_2), are less active under comparable conditions, specifically in a wet atmosphere.

Acknowledgements

This work is supported by the Senate of Berlin, Department for Urban Development, Environment and Technology and the European Fonds for Regional Development (Project 4086 ZÖW/C/O 40122/1). Mrs. R. Dambowsky, Mrs. S. Evert, Dr. D. Müller and Mr. U. Marx are thanked for sustained technical assistance. M. Richter and R. Fricke thank the Fond der Chemischen Industrie (VCI) for financial support.

References

[1] M. Richter, R. Eckelt, B. Parlitz, R. Fricke, Appl. Catal. B: Environm. 15 (1998) 129.
[2] M. Richter, B. Parlitz, R. Fricke, J. Chem. Soc., Chem. Commun., (1997) 383.
[3] F. Kapteijn, L. Singoredjo, A. Andreini, J.A. Moulijn, Appl. Catal. B: Environm. 3 (1994) 173.
[4] F. Kapteijn, A.D. van Langeveld, J.A. Moulijn, A. Andreini, M.A. Vuurman, A.M. Turek, J.M. Jehng, I.E. Wachs, J. Catal. 150 (1994) 94.
[5] F. Kapteijn, L. Singoredjo, M. van Driel, A. Andreini, J.A. Moulijn, G. Ramis, G. Busca, J. Catal. 150 (1994) 105.
[6] S. Kijlstra, J.C.M.L. Daamen, J.M. van de Graaf, B. van der Linden, E.K. Poels, A. Bliek, Appl. Catal. B: Environm. 7 (1996) 337.
[7] S. Kijlstra, D.S. Brands, E.K. Poels, A. Bliek, J. Catal. 171 (1997) 208.
[8] S. Kijlstra, D.S. Brands, H.I. Smit, E.K. Poels, A. Bliek, J. Catal. 171 (1997) 219.
[9] U. Lohse, I. Pitsch, E. Schreier, B. Parlitz, K.-H. Schnabel, Appl. Catal. A: Gen. 129 (1995) 189.
[10] W.M. Meier, D.H. Olson (Eds.), Atlas of Zeolite Structure Types, 4th revised ed., 1994, Butterworth Heinemann, 96 pp.
[11] Gmelins Handbuch der Anorganischen Chemie, 8. Auflage, Frankfurt/Main 1973, Mangan, Teil C1, 144 pp.
[12] E.P. Barrett, L.S. Joyne, P.P. Halenda, J. Am. Chem. Soc. 73 (1951) 373.
[13] W. Breck, Zeolite Molecular Sieves, Wiley, New York, 1974.
[14] I, W. Gerhartz (Ed.), Ullmann's Encyclopedia of Industrial Chemistry, 5th, completely revised version, vol. B2, Unit Operations, VCH, 1995, p. 2.
[15] J. Eng, C.H. Bartholomew, J. Catal. 171 (1997) 27.
[16] J. Eng, C.H. Bartholomew, J. Catal. 171 (1997) 14.